DENOISING OF THE DISTANCE DATA FROM UNDERWATER TIME-OF-FLIGHT (TOF) CAMERAS

Prashant Athavale[1†], *Kevin V. Mack*[1*], *Mahesh K. Banavar*[1*], *William D. Jemison*[1*], *David W. Illig*[2], *Luke K. Rumbaugh*[3], *Erik M. Bollt*[1*]

[1]Clarkson University, USA, [2]NAWCAD, USA, [3]Grove City College, USA

ABSTRACT

In underwater sensing, there is a demand for high-speed, high-resolution optical range imaging of objects in turbid water. Our prior work adapted commercially available time-of-flight (ToF) hardware to function in the unique optical conditions imposed by the water medium- namely, high levels of signal absorption and scattering. In this paper, we propose an algorithm to denoise the distance data captured with a ToF camera in turbid water conditions. To this effect, we use a 2-parameter scale-space generated by the iterative nonlocal means filter to denoise the DCS data. We then use these denoised DCS data to reconstruct the denoised distance image. We test the algorithm on data obtained from a simulated optical channel as well as real experimental ToF data. Compared with the local denoising methods, the results obtained with the proposed algorithm provide demonstrably improved distance images.

Index Terms— Time-of-Flight (ToF), underwater LiDAR, backscatter, underwater optics, denoising

1. INTRODUCTION

In underwater sensing and situational awareness, there is a need for high-resolution optical range imaging that can be used to identify objects in turbid water. Even at short range, underwater optical sensing is known to be challenging due to the heavy light scattering, and absorption induced by seawater [1]. A wide range of technologies with varying capabilities have been applied for such applications. These include consumer CCD cameras [2], laser line scanning systems with high-speed source driver circuits, and sampling rates on the order of GHz [2, 3]. Hardware solutions such as high-speed [4] or chaotic [5] intensity modulators, specialized optics [6,7], and beam shaping [8] methods have all been shown to mitigate the effects of light scattering in turbid water. In recent years, many have also found success by applying advanced signal processing algorithms to filter [9], deconvolve [10], or denoise [11] the received data. Furthermore, a combination of hardware or optical improvements aided by signal processing has also been effective [9, 12, 13].

In this work, we use an ESPROS epc660 ToF camera modified for underwater use and a custom flood illuminator with pulsed intensity modulation [14]. Images of an underwater scene are captured at varying levels of measured water clarity, or turbidity. An advantage of using the ToF camera is that it provides distance information from underwater objects. Since an underwater scene may have low contrast, the distance data obtained from the ToF camera is of particular interest.

Images obtained by the ToF camera described above are corrupted by blurring and shot noise [15]. In this paper, we introduce an algorithm based on a two-parameter scale-space to denoise the images obtained from the ToF camera. We note that denoising algorithms with such 2-parameter scale-space are not uncommon in image processing literature, a well-known example being the bilateral filter [16]. Furthermore, there exist numerous iterative denoising algorithms in the literature [17–19]. In particular, Wang et al. [20] propose iterative application of the nonlocal means filtering for salt-and-pepper denoising. We note that the parameter h is fixed in [20], which generates a single parameter scale-space. We demonstrate that for denoising underwater ToF data, the 2-parameter scale-space generated by the nonlocal means filter outperforms the compared local filtering methods.

The rest of the paper is organized as follows: Section 2 provides an overview of the ToF data demodulation and distance calculations. In Section 3, we propose the use of a 2-parameter scale-space, generated by the nonlocal means filter, for denoising. Section 4 discusses the results of the proposed algorithm on both synthetically generated (Section 4.1) and experimental ToF data (Section 4.2), for various levels of turbidity. We present concluding remarks in Section 5.

[†]Department of Mathematics, [*]Department of Electrical and Computer Engineering.

This work is supported by Office of Naval Research grant N00014-18-1-2291. Any opinions, findings, and conclusions or recommendations expressed in this material are those of the authors and do not necessarily reflect the views of the Office of Naval Research.

2. PROBLEM STATEMENT

The goal of this work is to denoise the ToF distance data that has been corrupted by the turbid underwater channel. The received signal, $x_R(t)$, is given by,

$$x_R(t) = I_o + I_{obj}\cos(2\pi f_{mod}t + \phi_{obj}) + I_{BS}\cos(2\pi f_{mod}t + \phi_{BS}), \quad (1)$$

where f_{mod} is the illuminator modulation frequency, ϕ_{obj} is the object induced phase shift, ϕ_{BS} is the phase shift due to the backscatter (BS), and I_o is the contribution from unmodulated and ambient light. I_{obj}, and I_{BS} are the intensity of the object and backscatter return, respectively. The ESPROS epc660 demodulates the received signal, $x_R(t)$, with four different demodulation signals. This results in four differential correlation sample (DCS) data, denoted d_i for $i \in \{0, 1, 2, 3\}$. These can be compared to the familiar IQ samples from RADAR literature [21] with $d_0 = T_{mod}Q, d_1 = -T_{mod}I, d_2 = -T_{mod}Q, d_3 = T_{mod}I$, and T_{mod} being the modulation period. Note that there are two samples from each channel, whose purpose is to help with hardware denoising and ambient light rejection. The distance value for each pixel can be computed from the DCS data by,

$$D = \frac{v}{2}\frac{1}{2\pi f_{mod}}\left[\pi + \arctan\left(\frac{d_2 - d_0}{d_3 - d_1}\right)\right] + d_{\textit{offset}}, \quad (2)$$

where v is the speed of light in water, f_{mod} is the source modulation frequency, and $d_{\textit{offset}}$ is a distance offset from a calibration step. In a low scattering scenario, the received signal in (1) is corrupted by shot noise proportional to I_{obj}. However, in turbid waters, the received signal is dominated by the backscatter return, burying the object in noise that is proportional to I_{BS}. This results in a loss of image contrast in addition to the forward scatter blurring, presenting a difficult image processing challenge. The noisy received signal can be written as,

$$\widetilde{x}_R(t) = x_R(t) + \eta(t, \lambda) \quad (3)$$

where $\eta(t, \lambda)$ is a Poisson distributed random variable parameterized by $\lambda = \text{var}\big(x_R(t)\big)$. As seen in (2) the distance data is proportional to the $arctan$ of the ratio $\left(\frac{d_2-d_0}{d_3-d_1}\right)$. When the data d_i are noisy, this results in more pronounced variations in the distance data, worsening the distance image quality. Hence, instead of denoising the distance image, we choose to denoise the 4 DCS data and use these denoised configurations to obtain the distance data.

3. PROPOSED ALGORITHM

In this section we introduce a 2-parameter scale-space for denoising. We describe, in order, preprocessing, our method to produce a 2-parameter scale-space, and how we use that for denoising the data.

3.1. Preprocessing

The magnitude of the noise in the data d_i is comparable to the received signal, resulting in outliers in the data. We define the outliers as data points whose values are more than 3 standard deviations away from the mean. We use the median filtering to remove these outliers, i.e we replace the outliers with median values of the neighbourhood values.

3.2. Producing a 2-parameter scale-space for nonlocal means filtering

The resulting data after pre-processing still needs denoising. The general idea behind denoising methods is to replace a given data point with a denoised value, which is often obtained based on its 'local' neighbourhood. Due to the low signal to noise ratio of the distance data, local denoising methods are not well suited for our application. Instead, we propose using nonlocal means filter [22, 23], where, given a data f on a domain $\Omega \subset \mathbb{R}^2$, a denoised image $NL[f](\cdot, h)$ is obtained using the following closed form equation:

$$NL[f](\boldsymbol{x}, h) = \frac{1}{C(\boldsymbol{x})}\int_\Omega e^{-\frac{G_a * \|f(\boldsymbol{x}+\cdot) - f(\boldsymbol{y}+\cdot)\|^2}{h^2}} f(\boldsymbol{y})\, d\boldsymbol{y}.$$

In the above equation $\boldsymbol{x} \in \Omega$, G_a is a Gaussian kernel with standard deviation a, h defines the degree of filtering, and $C(\boldsymbol{x})$ is the normalizing factor. This amounts to replacing every pixel in the given image f with the weighted mean of the values at points in its 'nonlocal' neighborhood. The parameter h affects the degree of smoothing. For a small value of the parameter h fewer pixels are included in the computation of the weighted nonlocal mean. On the other hand, for large value of h more number of pixels (potentially all pixels in the image) are considered in computing the mean. Buades et al. [22] use the parameter h as some multiple of the standard deviation, $\hat{\sigma}$, of the estimated noise, i.e. $h = \alpha\hat{\sigma}$.

3.3. Denoising the distance data

For the distance images obtained using the ToF camera the signal to noise ratio could be very low, and often negative for the individual DCS data. Thus, algorithms to estimate noise from the noisy data are often inaccurate. To circumvent this issue, we produce images $\{d_i^{\alpha,n}\}_{\alpha>0, n\in\mathbb{Z}_+}$ where α is a suitable multiplier of the estimation of the standard deviation of the noise, and n is the number of iterations. We note that $d_i^{\alpha,n}$ is oversmoothed if either α, or n is increased indefinitely. Thus, the family $\{d_i^{\alpha,n}\}_{\alpha>0, n\in\mathbb{Z}_+}$ describes a 2-dimensional scale-space, cf. [16, 17]. Hence, appropriate selection of α and n is needed. Once we obtain the denoised DCS data, we recover the denoised version of the distance data using (2). We describe this procedure in Algorithm 1.

Algorithm 1: Denoising the DCS data to obtain the distance image.

Preprocess the DCS data d_0, d_1, d_2, d_3 to eliminate the outliers (see section 3.1).
Compute $\hat{\sigma}^2(d_i)$, the estimate of the noise variance in the images d_i for $i = 1, \ldots 4$
Set $d_i^{\alpha,0} = d_i$ for $i = 1, \ldots 4$
for $i = 1$ *to* 4 **do**
  for $\alpha > 0$ *fixed* **do**
    for $j = 1$ *to* n **do**
      $d_i^{\alpha,j} = NL[d_i^{\alpha,j-1}](\cdot, \alpha\hat{\sigma}(d_i))$
    end
  end
end
Set $d_i = d_i^{\alpha,n}$ for $i = 1$ to 4.
Obtain the distance image D using (2).

4. RESULTS

We test our algorithm on both synthetic and experimental data to determine its effectiveness. We choose a subset of the turbidity levels from experiments in [14] for denoising. The selected levels are given in Table 1, which can also be used to relate attenuation lengths (AL) to measured turbidity. According to Beer's Law, the beam attenuation coefficient c describes the exponential power loss experienced when light propagates a certain distance z through the channel. The attenuation lengths given by $AL = cz$ is a useful way to compare experiments at different ranges and turbidity levels. We compare the results of the denoising algorithm on simulation data in Section 4.1. A depiction of the two-parameter scale-space is given in Fig. 1. The experimental results are given in Section 4.2. Simulation results can be compared to Fig. 2(a), while experimental results can be compared to Fig. 2(b). These images represent the object in clear water for the simulations and the experiments, respectively.

4.1. Results with synthetic data

We use the lighthouse image given in Fig.1(a) to demonstrate the 2-parameter scale-space produced by the nonlocal means filter. We add Poisson noise (also referred to as the shot noise) with $\lambda = 8000$ to the image Fig.1(a) resulting in Fig.1(b) with $SNR = -37.27\,dB$. Fig. 1(c-f) depict representative images in the 2-parameter scale-space of the nonlocal means filter.

We now demonstrate the denoising algorithm on a simulated object. To this effect, we simulate the blurring and backscatter induced by the underwater channel using the Waveform Response 3D (WR3D) simulator. WR3D is an analytic simulator which solves the radiative transfer equation and calculates the optical impulse response under a set of assumptions [24]. We add shot noise, with λ equal to signal

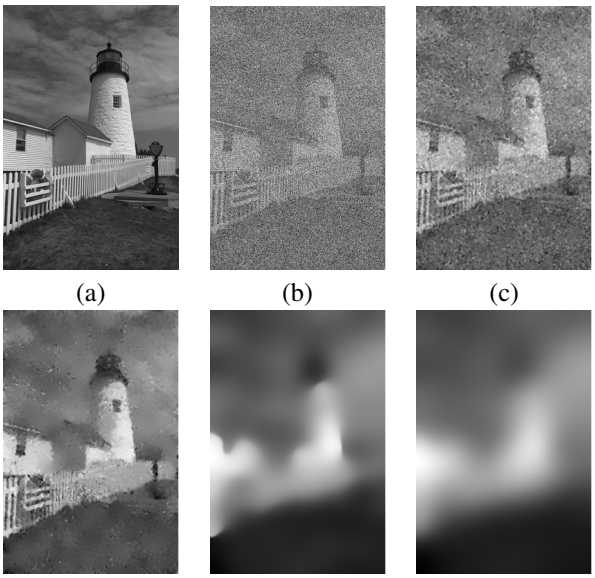

(a) (b) (c) (d) (e) (f)

Fig. 1. (a) Original image, (b) noisy image, (c) result of the algorithm for $\alpha = 0.6$, $n = 1$, (d) result of the algorithm for $\alpha = 0.6$, $n = 3$, (e) result of the algorithm for $\alpha = 0.6$, $n = 5$, (f) result of the algorithm for $\alpha = 0.6$, $n = 20$.

variance as in (3), to the output from WR3D, and emulate the hardware demodulation. The outcome is the simulated noisy DCS data, with resulting amplitude image given in Fig. 2(a) for clear water. As turbidity increases, the forward scatter blurring becomes more pronounced, as depicted in Fig. 3(a) with $AL = 14.98$ and no added noise. Fig. 3(b) shows the effect of added shot noise to Fig. 3(a), resulting in an SNR of $-0.37dB$. In Fig.3(f) we see the result of the proposed algorithm on the distance data shown in Fig. 3(b). In the case of synthetic data, the proposed algorithm was more effective in denoising the distance data than local denoising methods, such as bilateral filter [16], TV denoising [25], and TV flow denoising [26] as seen in Fig. 3(c), (d), and (e), respectively. Though blurring from forward scattered light is still present,

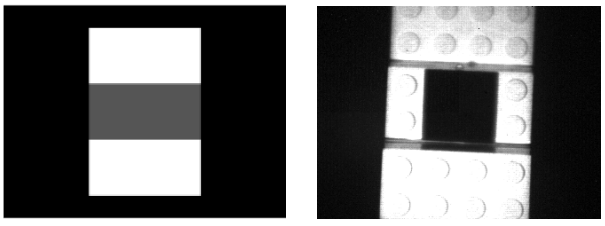

(a) (b)

Fig. 2. (a) Simulated object in clear water $AL = 0.03$, (b) image of object from $AL = 0.74$ in the experimental dataset. Note that both clear water images have good contrast and no noticeable blurring.

Measured c (m^{-1})	Attenuation Lengths (AL)
1.233	0.740
3.128	1.877
6.113	3.668
8.956	5.373
14.355	8.613
24.972	14.983

Table 1. Select experiment parameters from our previous work

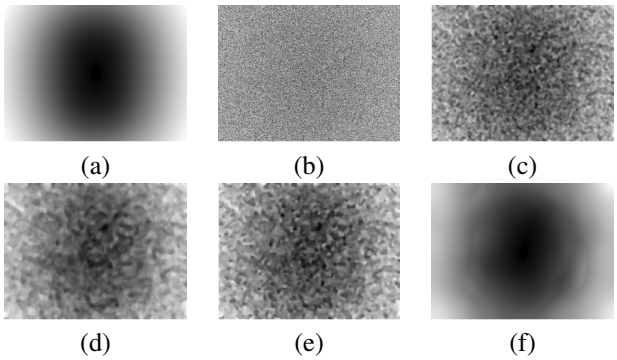

Fig. 3. (a) Original synthetic distance image at $AL = 14.98$, (b) distance image with simulated noise added, (c) result of the bilateral filter, (d) result of the TV regularization with $\lambda = 1$, (e) result of the TV flow, (f) result of the proposed algorithm for $\alpha = 4, n = 8$.

the shot noise has effectively been removed.

4.2. Results with experimental ToF data

In Fig. 4 we see the results of the algorithm on real underwater distance data obtained from the ToF camera. The experiments were performed in a small-scale test tank with the adapted ToF camera and a 4 cm tall object at a standoff distance of 0.7 m. More details about the experiment can be found in [14]. We select a subset of the turbidity levels from these experiments for denoising. The distance images displayed in Fig. 4 (a), (c), and (e) represent the raw noisy images taken at $AL = 3.67, AL = 5.37$, and $AL = 8.61$, respectively. The denoised images, Fig. 4 (b), (d), and (f) show a clear improvement and denoising of the underwater object, without causing any further blurring of the edge features.

5. CONCLUSIONS

In this paper, we proposed an algorithm for denoising DCS data and reconstruct the distance data, via a 2-parameter scale-space using nonlocal means. We compared the proposed algorithm to other established techniques by denoising

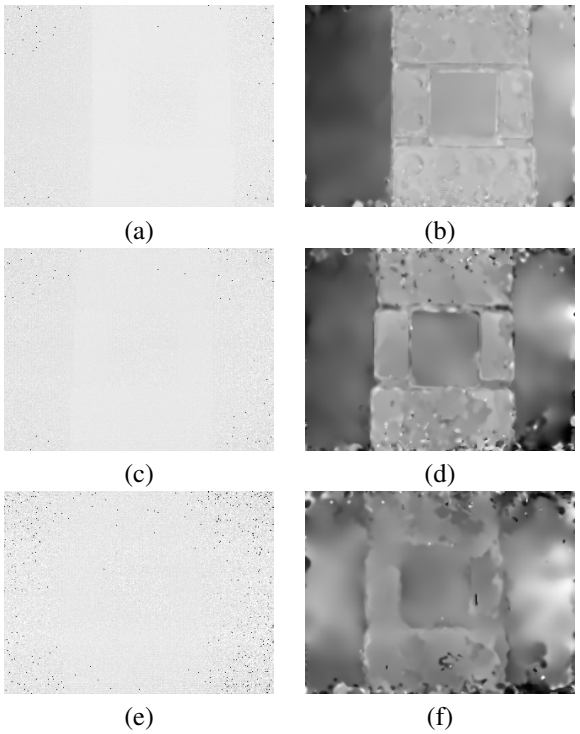

Fig. 4. (a) Distance image obtained from the experimental setup with $AL = 3.67$ and (b) result of the algorithm, (c) Distance image obtained from the experimental setup with $AL = 5.37$ and (d) result of the algorithm, (e) Distance image obtained from the experimental setup with $AL = 8.61$, (f) result of the algorithm. For all cases the algorithm used $\alpha = 2, n = 5$.

synthetically generated DCS data. In this work the value of the parameters α and n were empirically chosen. In our future work, we aim to automate the selection of these parameters. We also aim to test this algorithm on a new experimental dataset, which will be captured at the large-scale testing facility at Clarkson University, which allows for object standoff distances of up to 8 meters.

6. REFERENCES

[1] F. M. Caimi, D. M. Kocak, F. Dalgleish, and J. Watson, "Underwater imaging and optics: Recent advances," in *OCEANS 2008*, Sept. 2008, vol. 2008-Supplement, pp. 1–9, ISSN: 0197-7385.

[2] J. S. Jaffe, "Underwater Optical Imaging: The Past, the Present, and the Prospects," *IEEE Journal of Oceanic Engineering*, vol. 40, no. 3, pp. 683–700, July 2015.

[3] L. J. Mullen and V. M. Contarino, "Hybrid LIDAR-radar: Seeing through the scatter," *IEEE Microwave Magazine*, vol. 1, no. 3, pp. 42–48, Sept. 2000.

[4] L. Mullen, A. Laux, B. Concannon, E. P. Zege, I. L. Katsev, and A. S. Prikhach, "Amplitude-modulated laser imager," *Applied Optics*, vol. 43, no. 19, pp. 3874–3892, July 2004.

[5] L. K. Rumbaugh, E. M. Bollt, W. D. Jemison, and Y. Li, "A 532 nm chaotic lidar transmitter for high resolution underwater ranging and imaging," in *2013 OCEANS - San Diego*, Sept. 2013, pp. 1–6, ISSN: 0197-7385.

[6] A. Jantzi, W. Jemison, D. Illig, and L. Mullen, "Axicons for improved lidar performance," in *Ocean Sensing and Monitoring XII*. Apr. 2020, vol. 11420, p. 114200A, International Society for Optics and Photonics.

[7] S. Panigrahi, J. Fade, R. Agaisse, H. Ramachandran, and M. Alouini, "An all-optical technique enables instantaneous single-shot demodulation of images at high frequency," *Nature Communications*, vol. 11, no. 1, pp. 549, Dec. 2020.

[8] A. Jantzi, W. Jemison, A. Laux, L. Mullen, and B. Cochenour, "Enhanced underwater ranging using an optical vortex," *Optics Express*, vol. 26, no. 3, pp. 2668–2674, Feb. 2018, Publisher: Optical Society of America.

[9] D. M. Kocak, F. R. Dalgleish, F. M. Caimi, and Y. Y. Schechner, "A Focus on Recent Developments and Trends in Underwater Imaging," *Marine Technology Society Journal*, vol. 42, no. 1, pp. 52–67, Mar. 2008.

[10] D. W. Illig, L. K. Rumbaugh, M. K. Banavar, and W. D. Jemison, "Blind signal separation for underwater lidar applications," *AIP Conference Proceedings*, vol. 1757, no. 1, pp. 060003, 2016.

[11] B. Ouyang, F. R. Dalgleish, F. M. Caimi, A. K. Vuorenkoski, T. E. Giddings, and J. J. Shirron, "Image enhancement for underwater pulsed laser line scan imaging system," in *Ocean Sensing and Monitoring IV*. June 2012, vol. 8372, p. 83720R, International Society for Optics and Photonics.

[12] B. Ouyang and W. Hou, "Compressive line sensing imaging system in a controlled hybrid scattering environment," *Optical Engineering*, vol. 58, no. 02, pp. 1, Feb. 2019.

[13] D. W. Illig, L. K. Rumbaugh, M. K. Banavar, E. M. Bollt, and W. D. Jemison, "Backscatter suppression via blind signal separation for a 532 nm underwater chaotic lidar rangefinder," in *OCEANS 2015 - MTS/IEEE Washington*, Oct. 2015, pp. 1–6.

[14] K. V. Mack, W. D. Jemison, L. K. Rumbaugh, D. W. Illig, and M. K. Banavar, "Time-of-Flight (ToF) Cameras for Underwater Situational Awareness," in *OCEANS 2019 MTS/IEEE SEATTLE*, Oct. 2019, pp. 1–5, ISSN: 0197-7385.

[15] W. Schottky, "On spontaneous current fluctuations in various electrical conductors," *Journal of Micro/Nanolithography, MEMS, and MOEMS*, vol. 17, no. 4, pp. 041001, Oct. 2018, Publisher: International Society for Optics and Photonics.

[16] C. Tomasi and R. Manduchi, "Bilateral filtering for gray and color images," in *Sixth international conference on computer vision (IEEE Cat. No. 98CH36271)*. IEEE, 1998, pp. 839–846.

[17] E. Tadmor, S. Nezzar, and L. Vese, "A multiscale image representation using hierarchical (BV, L^2) decompositions," *Multiscale Modeling & Simulation*, vol. 2, no. 4, pp. 554–579, 2004.

[18] E. Tadmor, S. Nezzar, and L. Vese, "Multiscale hierarchical decomposition of images with applications to deblurring, denoising and segmentation," Tech. Rep., University of Maryland, College Park., 2007.

[19] P. Athavale and E. Tadmor, "Integro-Differential Equations Based on (BV, L^1) Image Decomposition," *SIAM Journal on Imaging Sciences*, vol. 4, no. 1, pp. 300–312, 2011.

[20] X. Wang, S. Shen, G. Shi, Y. Xu, and P. Zhang, "Iterative non-local means filter for salt and pepper noise removal," *Journal of visual communication and image representation*, vol. 38, pp. 440–450, 2016.

[21] M. I. Skolnik, *Radar Handbook, Third Edition*, McGraw-Hill Education, 2008.

[22] A. Buades, B. Coll, and J-M Morel, "A non-local algorithm for image denoising," in *2005 IEEE Computer Society Conference on Computer Vision and Pattern Recognition (CVPR'05)*. IEEE, 2005, vol. 2, pp. 60–65.

[23] A. Buades, B. Coll, and J-M Morel, "A review of image denoising algorithms, with a new one," *Multiscale Modeling & Simulation*, vol. 4, no. 2, pp. 490–530, 2005.

[24] E.P. Zege, A.P. Ivanov, and I.L. Katsev, *Image Transfer Through a Scattering Medium*, Springer-Verlag, 1991.

[25] L. I. Rudin, S. Osher, and E. Fatemi, "Nonlinear total variation based noise removal algorithms," *Physica D: nonlinear phenomena*, vol. 60, no. 1-4, pp. 259–268, 1992.

[26] V. Caselles, A. Chambolle, and M. Novaga, "The discontinuity set of solutions of the tv denoising problem and some extensions," *Multiscale modeling & simulation*, vol. 6, no. 3, pp. 879–894, 2007.